ResearchGate

See discussions, stats, and author profiles for this publication at: https://www.researchgate.net/publication/268572163

# Auxiliary Power Unit Compartment Design Optimization

**Conference Paper** · September 2012

DOI: 10.2514/6.2012-5710

CITATION
1

READS
2,648

**3 authors**, including:

Ohad Gur

**44** PUBLICATIONS **1,026** CITATIONS

SEE PROFILE

All content following this page was uploaded by Ohad Gur on 30 July 2015.

The user has requested enhancement of the downloaded file.

# Auxiliary Power Unit Compartment Design Optimization

**Ohad Gur[1], Jonathan Lewis[2], and Gali Lazar[3]**

**IAI - Israel Aerospace Industries**

## Abstract

**In this paper a design process of auxiliary power unit (APU) compartment is presented. This design effort incorporates several disciplines and models. The design goal is to comply with the temperature level constraints, mass flow requirements, and reduce to minimum the drag penalty. The proposed method enables the cooperation of several stand-alone models which are integrated into a comprehensive design framework using ESTECO modeFRONIER environment. A bi-level design process was developed to enable minimum effort of updating the high fidelity model. Most of the design process is done using the low fidelity models, thus enabling a thorough study of the design space with low computer resources. Then, a validation process is conducted using the high fidelity model. The results prove the validity of the proposed method with reduction of the drag penalty and decreased temperature level below the required limits. The activity is part of the GTA (Global Thermal Aircraft) effort in CRESCENDO (Collaborative & Robust Engineering using Simulation Capability Enabling Next Design Optimization) European-Union Seventh Framework Program.**

## Nomenclature

$A_1$ = inlet area
$A_2$ = APU-engine inlet area
$A_6$ = APU-engine nozzle area
$A_8$ = APU-compartment cross section area
$A_9$ = APU-compartment area at the plane defined by the APU-engine nozzle
$A_e$ = inlet outer wetted area
$C_{L\max}$ = aircraft maximum lift coefficient
$D_1$ = inlet height
$D_{1E}$ = inlet external height
$F_{\text{Orifice}}$ = orifice ratio – ratio of inlet area used by the APU-compartment
$\mathbf{f}$ = cost function array
$g$ = design constraint
$H$ = altitude
$j$ = index
$L_{fairing}$ = fairing length
$L_{mix}$ = ejector mixing length
$M$ = Mach number
$S_{wing}$ = wing area
$T$ = temperature
$T_{\max}$ = maximum allowed temperature

---

[1] Preliminary design department, ogur@iai.co.il , AIAA Member
[2] Heat-transfer department, jlewis@iai.co.il
[3] Preliminary design department, glazar@iai.co.il

$T_{ratio,\max}$ = maximum normalized temperature ratio
$V_{compartment}$ = APU-compartment volume
$V_{SL,ISA}$ = maximum allowed velocity at sea level ISA conditions
$W$ = weight
$W_1$ = inlet width
$W_{1E}$ = inlet external width
$\mathbf{x}$ = design variables vector
$\delta_0$ = total pressure ratio
$\theta_0$ = total temperature ratio

# I. Introduction

In nowadays air-vehicles development, integrating the auxiliary power unit (APU) is a complex design challenge. APU is an additional engine which fills the following purposes in a modern designed air-vehicle:

a. Providing power to start the main engines.
b. Running accessories while the engines are shut down.
c. Providing electrical & hydraulically (depending on the design) power before engine start (pre-flight tests, cabin ventilation, ect.).

These duties emphasize the APU importance as a critical system. Thus, it should comply with restrictive design constraints. First, its reliability demands are high, thus its availability is required at different demanding conditions such as emergency cases or during takeoff. Second, its installation and operation should not interfere with the normal air-vehicle operation. This indicates a demand for small dimension, and minimum drag penalty design. Moreover, in most cases, the APU is buried inside the aft part of the fuselage, thus, contrary to the aircraft main engines (which are located in the free stream), the produced heat should be efficiently removed from the APU compartment. Figure 1 shows such an installation in a business jet empennage section. The paper deals with such design problem and presents an optimized design approach for APU compartment.

Large effort is invested in APU-engine design. Interesting example is the space shuttle APU design. [1] In its description the true multidisciplinary nature of the entire APU program, especially for space usage, is revealed. The multiple systems such as control, turbine, gear box, heat exchangers, etc., shed light on the complexity of the design task. An additional example for APU modeling is given by Gorinevsky et-al. [2] In their paper a design of diagnostic system for APU turbine system is considered. The design is done using a detailed APU model which includes a gearbox, load compressor, power section, and exhaust model, along with other components such as starter model, fuel controller etc.

As mentioned above the purpose of the current effort is not to design the APU-engine but to design its installation compartment. Two important aspects are the design of the APU ejector and the compartment inlet.

The ejector is the mixing area which joins the APU-engine exhaust gases and the APU-compartment flow. Two main inlet configurations are available: joint and separate. The joint inlet feed both the APU engine and the APU-compartment while the separate consists of two inlets, one for the APU-engine and the other for the APU-compartment.

The purpose of the ejector is to ensure that a steady flow of air exists in the APU compartment and to maintain the temperature level of the hot exhaust gases. Ordonez and Georges [3] review the importance of the ejector design and its influence over the air vehicle performance such. Jesus and Oliveira [4] showed the importance of proper inlet design for both mass flow requirements and low drag penalties.

These examples point that the APU integration design process consists of several disciplines: propulsion simulation, heat transfer, inlet aerodynamics, and air-vehicle performance. All of these disciplines should be taken into consideration as a unified design framework, thus a MDO (Multidisciplinary Design Optimization) approach can be used.

In the current effort, which consists of several different analyses, two separate preliminary design procedures are presented:

a. For a given APU compartment, a search process is conducted to find the critical flight condition, which reflects the most demanding condition for a given APU.
b. For a given flight condition, a preliminary design of an APU compartment is conducted. This includes the inlet, exhaust, and ejection geometries, and done with minimum drag penalty along with mass flow constraints.

These two search procedures are then interconnected into a unified design loop which results with compartment design for critical flight conditions.

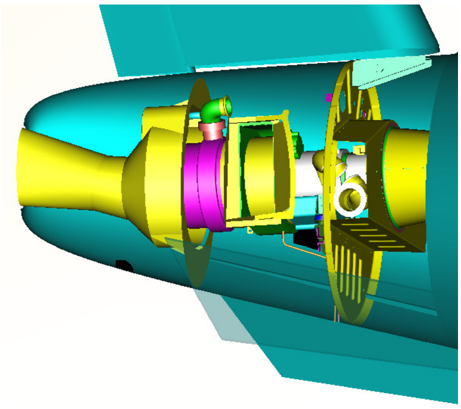

**Figure 1. APU drawing as part of the empennage section of an air-vehicle**

## II. Design Problem Description

APU compartment design can be described as a search problem (or mathematical programming problem) which quests the optimal geometric properties of the APU. Design goals are imposed on the problem along with several design constraints, thus a multi-objective optimization problem is defined. This optimization problem can be defined using standard formulation. Equation (1) contains such a formulation, where **f**(**x**) is the cost function array (design goals), **x** is a set of design parameters (variables), and $g_j$ are the design constraints.

$$\begin{aligned} &\min_{\mathbf{x}\in\Re^n} \mathbf{f}(\mathbf{x}) \\ &\textit{Subject to} \quad g_j \le 0,\ j = 1,2,\ldots m \end{aligned} \tag{1}$$

For each design problem one should define the above mentioned parameters: design variables, design goal, and design constraint. In the current scope the plenary design problem can be defined as follows:

a. The design variables are the APU compartment geometry and flight conditions. The geometry design variables include the inlet, APU chamber, and ejector geometry definitions. The flight conditions are the most critical condition for the APU compartment design.
b. The design goal is to minimize the drag penalty due to the inlet presence. Increased inlet dimensions enables sufficient mass flow, thus the APU chamber will maintain its temperature level. On the other hand, increased inlet dimensions may lead to high drag penalty, which deteriorates the air vehicle performance.
c. The main design constraint is the temperature level which should be confined below a certain limit. This ensures a safe operation of the air-vehicle.

This design problem contains several different analyses. The unified plenary process of these analyses under the above goals and constraints is presented in Fig. 2. For a given set of design variables (*i.e.* flight condition and geometry), inlet, 1-D flow model, ejector, and a given APU-engine, one can find the boundary conditions for the thermal analysis. These boundary conditions contain the total mass flow through the compartment, the APU-engine mass flow, APU-engine temperature, and the pressure recovery of the inlet. These boundary conditions are used by the thermal model to find the temperature distribution in the APU compartment. The temperature distribution is then used as a design constraint. The inlet drag penalty is used as a design goal.

As part of the design process, an optimizer updates the design variable: flight conditions and geometry parameters. Critical flight conditions are searched, thus the most conservative conditions are used. In addition the geometry is updated, thus the minimum drag penalty is found along with a feasible temperature solution – the temperature limits are preserved.

Dealing with such a complex design problem forces the designer to break the plenary design scheme into bi-level process, which enables a practical and flexible solution. Figure 3 exhibits the two steps design scheme. The left hand part of the figure shows similar components which also exist in the plenary problem (Fig. 2). The major difference involves the optimizer functionality. While for the plenary process the optimizer searches for both the design-conditions and geometry parameters, in the bi-level scheme the first step process searches only for the critical flight conditions. The resulted flight conditions represent the most severe condition which derives a critical temperature distribution. This means that Step-I part run without updating the APU compartment geometry (thermal model). Thus, the high fidelity thermal model is not required to be re-meshed.

Step II, as presented on the left hand part of Fig 3, contains only the APU-engine, inlet, and ejector models. On these models the geometry optimization is conducted, namely the minimum drag configuration is found. These models demand low computer resources, thus the geometry optimization process is relatively simple.

After optimizing the geometry, for the most severe conditions, the process is repeated with step I starting with the new improved geometry. Note that just in this transition (*i.e.* from the solution of step II to re-run of step I) the thermal model geometry is regenerated. In most of non-exotic cases, this single thermal model updated is enough. The validation for that argument is if the same critical flight condition is kept. In this case re-running step II is unnecessary. In addition, the need of thermal model geometry updates is confined to a single perturbation. This makes the need for thermal-model automatic meshing redundant.

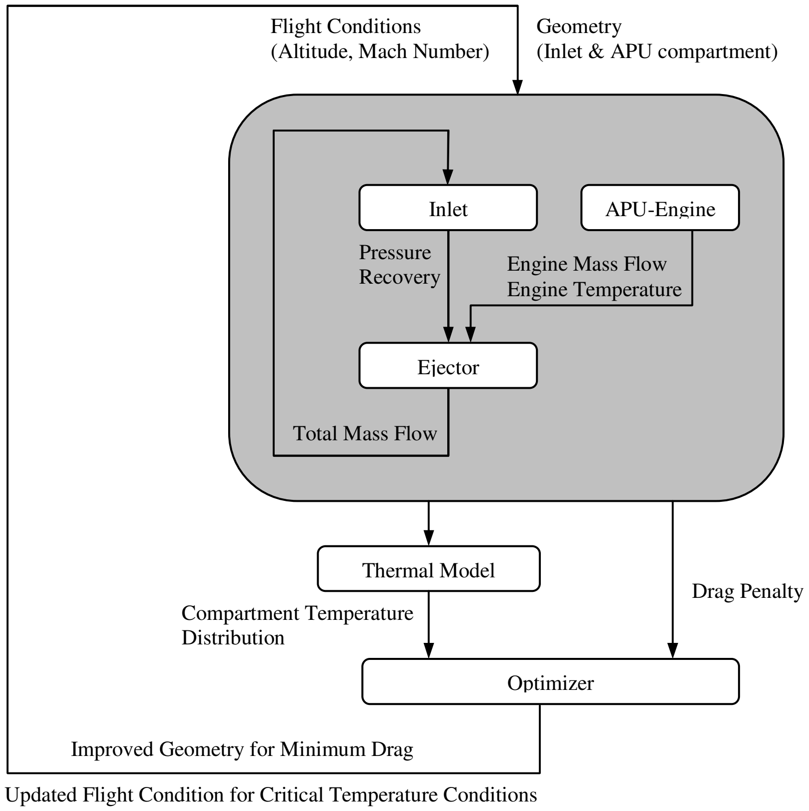

**Figure 2. Plenary design problem scheme**

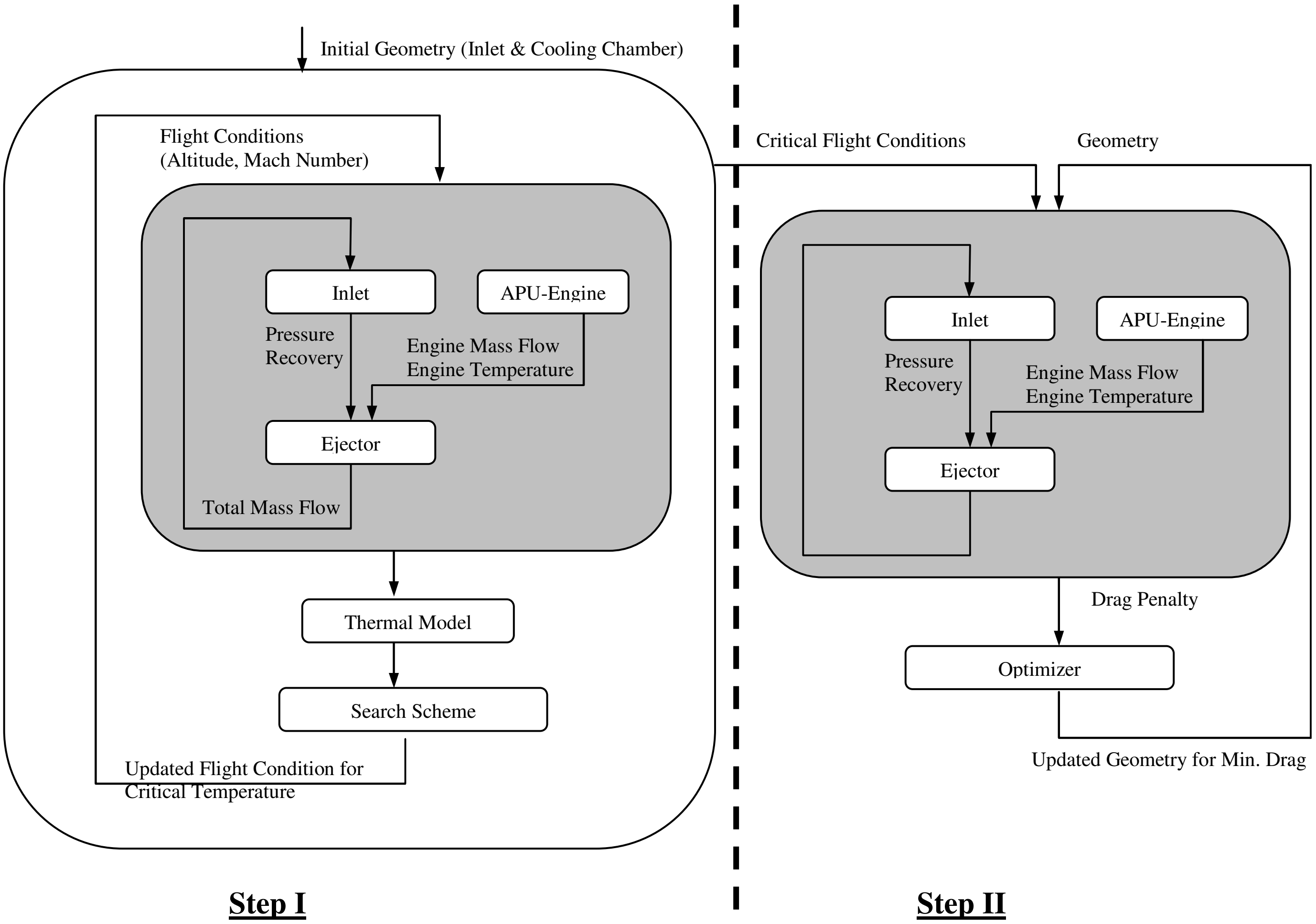

**Figure 3. Separated design problem scheme**

## III. Design Framework

Two design frameworks were constructed for the current effort. These frameworks reflect step I and step II parts presented in Fig. 3. As stated above, the purpose of the first framework is to find the critical flight conditions for a given geometry and the purpose of the second framework is to find an optimal design for given flight condition.

Both frameworks are base on four models, each implemented differently and based on different analysis:

a. Inlet model
b. Ejector model
c. Thermal model
d. APU-engine model

A detailed description of each model is given in the following sub-sections.

The various models, for the two frameworks, are integrated using ESTECO modeFRONTIER® environment. This design environment enables an integration of different models and enables the usage of various optimization procedures.

Figure 4 shows the critical flight condition search framework which is the representation of Stage-I in Fig. 3. It contains the inlet APU-engine and ejector models. Although the APU model is not visible it is part of the ejector sub-system appear in Fig. 4. These 3 models supply the boundary condition for the thermal model which calculates the temperature of the APU compartment components.

Figure 5 shows the implementation of the inlet and exhaust (again, the APU-engine model is inside the ejector sub-system). This framework is used for the optimization of the APU compartment and inlet geometry, i.e. implementation of Stage-II in Fig. 3 .

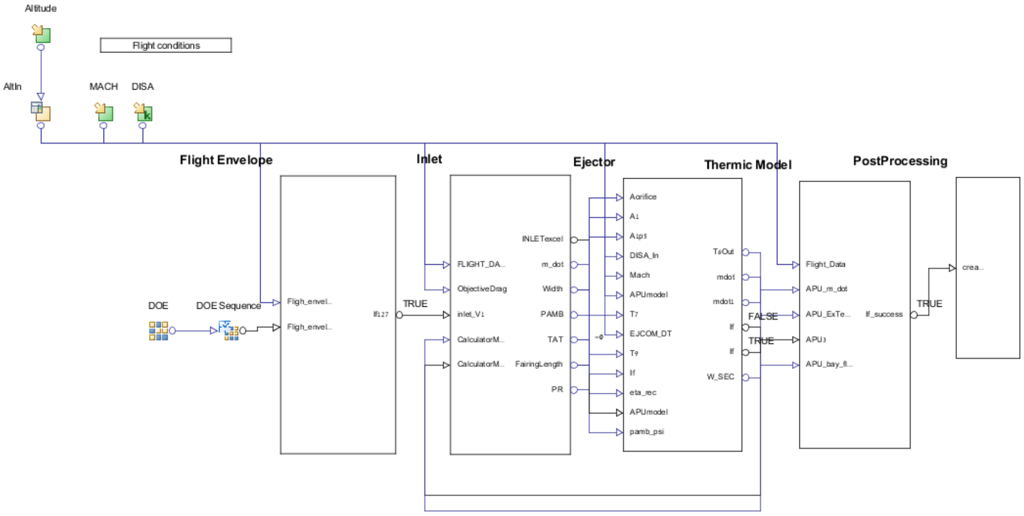

**Figure 4. Critical flight condition search design framework (Step-I) using ESTECO-modeFRONTIER**

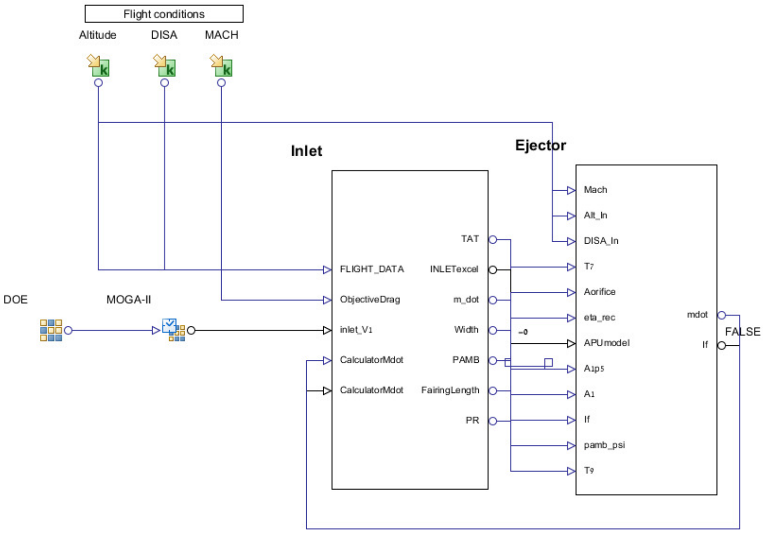

**Figure 5. Inlet-ejector geometry optimization design framework (Step-II) using ESTECO-modeFRONTIER**

## A. Inlet model

The inlet model is required to estimate the drag penalty on the air vehicle and the pressure recovery of the inlet. These are found as a function of the inlet mass flow. The analysis is based on empirical models, which fits various inlet type, *e.g.*, NACA scoop scoops with or without diverter, etc. The model is presented in ESDU-86002 data sheet.[6]

For the current effort a rectangular scoop is used which is defined using the inlet height, $D_1$, and inlet width, $W_1$ (see Fig. 7). Other geometry properties are derived from these two parameters.

The inlet external height, $D_{1E}$, and external width, $W_{1E}$ are related to the inlet height and width, through the following relation:

$$\begin{aligned} D_{1E} &= D_1 + 0.005\,m \\ W_{1E} &= W_1 + 0.01\,m \end{aligned} \tag{2}$$

Thus, the inlet skin thickness is estimated as 0.005 m.

The inlet area is the product of its width and length:

$$A_1 = D_1 \cdot W_1 \tag{3}$$

The inlet is considered to be placed 20 m from the fuselage nose, thus it experiences a fully developed boundary layer. The fairing length, $L_{fairing}$ is set to a constant value of $L_{fairing} = 0.2$ m . The inlet outer wetted area $A_e$, is calculated by the following relation:

$$A_e = 1.2W_1\sqrt{D_1^{\,2} + L_{fairing}^{\,2}} \tag{4}$$

In the above manner, the entire inlet geometry is defined using just its width and height.

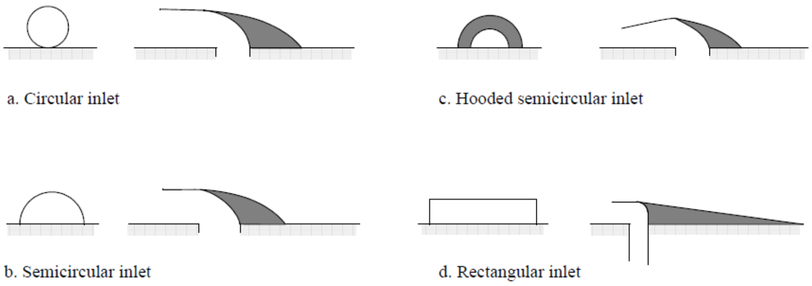
a. Circular inlet

c. Hooded semicircular inlet

b. Semicircular inlet

d. Rectangular inlet

**Figure 6. Example of inlet types** [6]

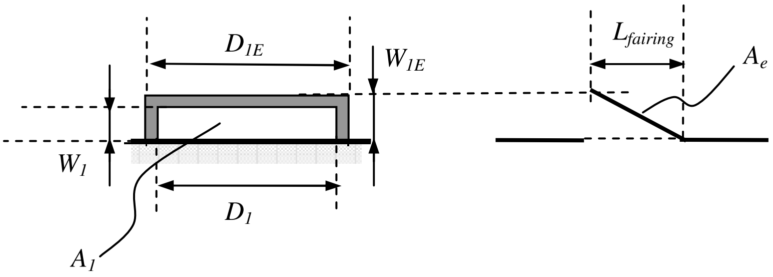

**Figure 7. Rectangular inlet geometric definition**

## B. APU-Engine Model

The AUP-engine model estimates the mass flow through the APU-engine and the temperature at the APU nozzle. These properties are then used by the thermal model of the APU compartment as an input. The APU model is based on genuine steady-state engine deck software. The engine deck is replaced with characterization curves depending only on the ambient conditions of $\delta_0\sqrt{\theta_0}$, where $\delta_0$ and $\theta_0$ are the stagnation pressure and temperature ratios, respectively. Figure 8 shows the APU-engine model curves for two temperature conditions, ISA and ISA+35 Centigrade. The output APU-engine temperature has a distinctive step shape which is due to the bleed valves logic which depends on the flight conditions. This step characteristic has a great influence over the operation envelope of the APU compartment.

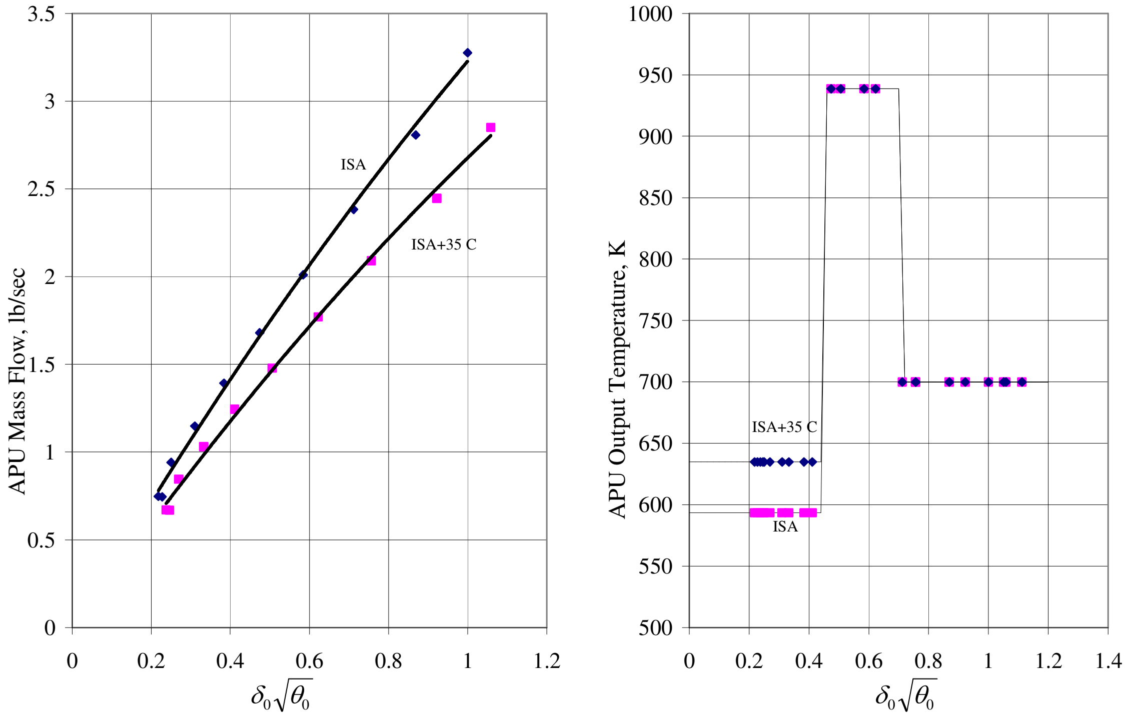

**Figure 8. APU-engine model**

### C. 1-D flow and Ejector Model

The 1-D flow and ejection model supplies the APU-engine and APU compartment integration as a 1-D flow analysis described in Ref. 7. The purpose is to model this complex mutual interference as a simplified model which can be defined through small number of design variables. This is in contrary to the thermal model which is considered in the current scope as a high fidelity model.

Figure 9 presents the geometry of the APU compartment including the APU-engine and the inlet geometry. Figure 10 presents a schematic view of a similar APU compartment for separate-inlet configuration APU. In this configuration the air entering the APU engine (station 1) has a separate inlet than the air entering the APU compartment (station 7). The two flows intersect at the APU engine nozzle (station 6), mixed, and then emitted through a joint diffuser (station 10). The joint inlet APU compartment is similar except of the absence of station 7 (the separate compartment inlet in Fig. 10).

The simplified 1-D model enables modeling the problem through the use of low number of parameters. These parameters define the geometry of the stations along the air path. In the current effort a joint inlet configuration is used with the following design variables:

a. Nozzle area, $A_{10}$
b. Mixing length, $L_{mix}$
c. The orifice ratio, $F_{\text{Orifice}}$. It is defined as the ratio of the inlet area which is used by the APU compartment:

$$F_{\text{Orifice}} = \frac{A_1 - A_2}{A_1} \tag{5}$$

where $A_1$ is the joint inlet area and $A_2$ is the APU-engine inlet area (see Fig. 11).

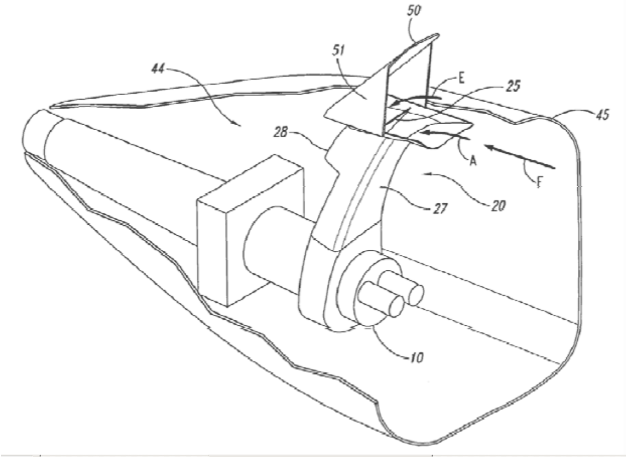

Figure 9. Geometry of the APU compartment. In this figure a separate inlet configuration is described. [8]

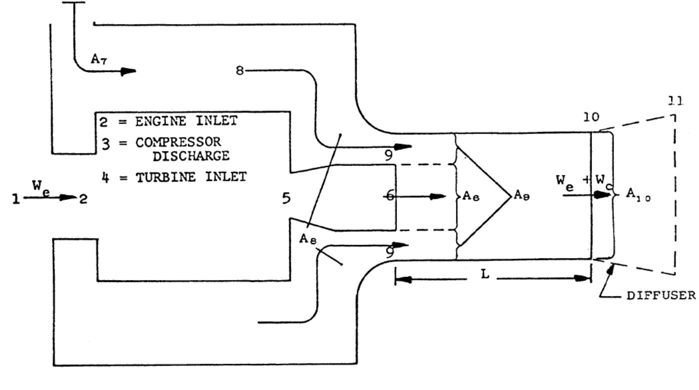

Figure 10. Schematic of the geometric properties of a separate inlet ejector. [7]

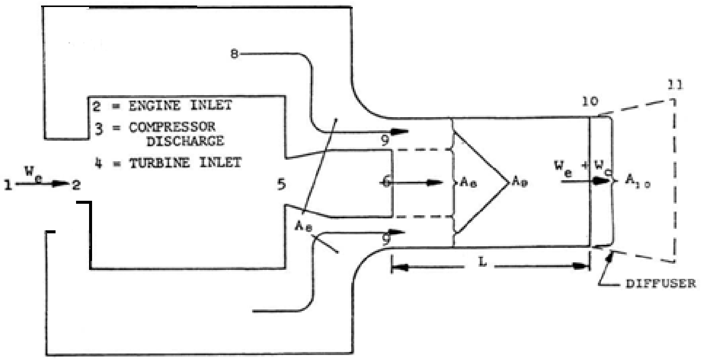

**Figure 11. Schematic of the geometric properties of a joint inlet ejector.** [7]

Note that except of these 3 parameters, one can use any other parameter as a design variable, *e.g.* APU compartment volume, $V_{compartment}$, APU compartment cross section area, $A_8$, etc. For the current scope, all other parameters are considered fixed as defined in Table 1.

**Table 1. APU compartment fixed geometric parameters**

| Parameter | Value |
|---|---|
| $A_6$ | $D_6 = 0.32$ m , $A_6 = 0.0804$ m$^2$ |
| $A_{10}$ | $D_{10}= 0.38$ m ,$A_{10} = 0.1134$ m$^2$ |
| $A_9$ | $A_9 = A_{10} - A_6 = 0.033$ m$^2$ |
| $A_8$ | $A_8 = 10\ (A_{10} - A_6) = 0.33$ m$^2$ |
| $V_{compartment}$ | 12 ft$^3$, 0.34 m$^3$ |

### D. Thermal Model

The thermal model is considered as a high fidelity model. It contains the flow and thermal model for a predefined inlet, exhaust, and ejection geometry and it is based on MSC-Patran meshing and MSC-Sidna solver. In the developed design process, the thermal model geometry is changed only once. This is done after the ejector geometry is optimized, and a new optimized APU compartment geometry is found. By confining the optimization to the simplified ejector model, rather to the high fidelity thermal model, enable the designer to use a single perturbation over the high fidelity analysis, *i.e.* thermal model. Although this introduces some inaccuracies, it gives a rapid and easy method of designing an APU compartment.

Figure 12 presents the initial baseline geometry implemented in MSC-Patran mesh generator. This geometry is taken from the GTA (Global Thermal Aircraft) configuration which is part of the CRESCENDO (Collaborative & Robust Engineering using Simulation Capability Enabling Next Design Optimisation) project. Entire structure of the aft fuselage section is modeled including the skin, ribs, and stringers. The APU engine and the APU compartment with its inlet and nozzles are modeled as well.

The boundary conditions, namely the mass flow, APU engine exhaust temperature, and inlet ram recovery are estimated using the APU-engine and inlet models. This enables to implement the thermal model in an analysis (rather than design) framework, thus finding the critical flight conditions within the air vehicle flight envelope.

At each flight condition, the thermal model can be solved and the temperature distribution for its components is found. Figure 13 shows a graphic representation of such solution. The hot temperature along the mixing length, at the exhaust of the APU-engine is visible. The nozzle hot air flow is also visible along with the hot jet influence on the outer skin temperature.

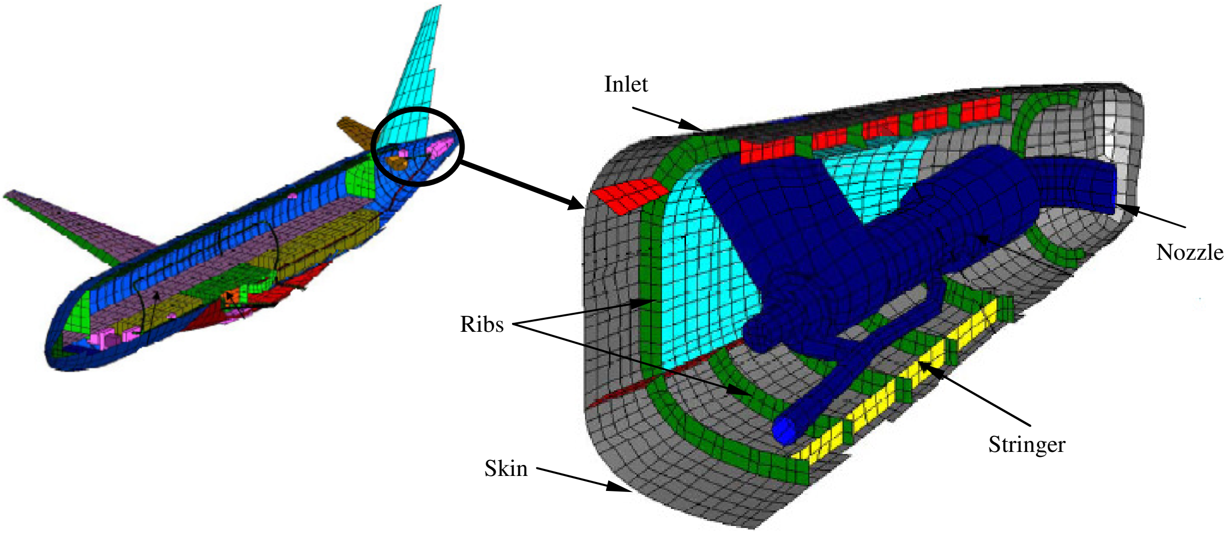

**Figure 12. Compartment baseline geometry**

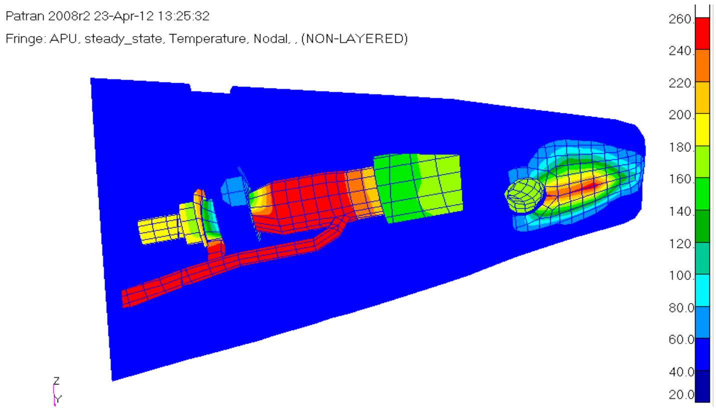

**Figure 13. Thermal model solution**

The thermal model results with the temperature distribution of the model nodes, thus the maximum temperature for each material can be found (the model consists of several materials). Table 2 contains the various materials which include in the APU compartment. For each material the upper and lower temperature limits are stated. Note that for air, an altitude dependent model based on a Military-Standard [9] is used (see Fig. 14).

**Table 2. Nominal parameters of inlet and ejector for the critical conditions calculation**

| Material | Max. Temp. Limit Centigrade |
|---|---|
| Aluminum | 160 |
| Titanium | 300 |
| Bay Flow | Altitude dependent model |

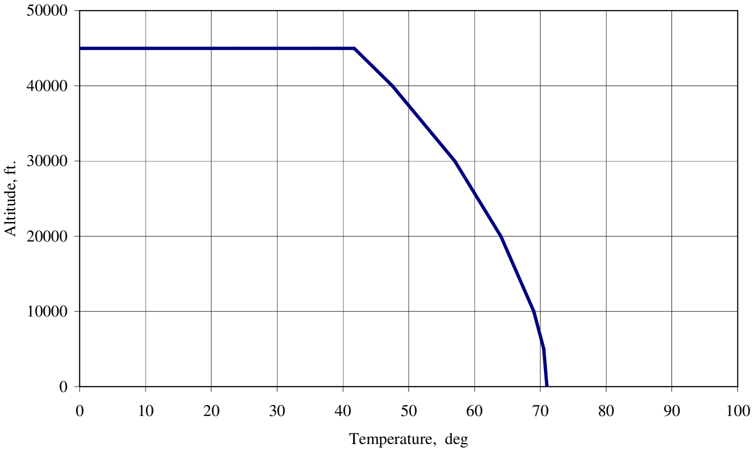

**Figure 14. temperature limit model for air** [9]

To evaluate the most critical condition, temperature ratios are used. Maximum normalized temperature ratio is defined, $T_{ratio,max}$. at each node, according to the following relation:

$$T_{ratio,\max} = \frac{T - T_{\max}}{T_{\max}} \tag{6}$$

$T$ is the temperature at the node and $T_{max}$ is the maximum temperature limit of the node material, taken from Table 2.

In this manner, all the nodes can be compared, thus if a positive ratio is resulted, the temperature limit is exceeded. From all calculated temperature ratios, one can find the highest ratio for each flight condition.

## IV. Design Cycle Demonstration

The design cycle of an APU compartment is demonstrated using the bi-level process described above. The first step is estimating the critical flight condition for a given initial design. Then, the critical flight conditions are used for an optimization of the APU compartment geometry. Finally, the optimized design is being validated through re-running the first step.

As mentioned above, the results presented in the following sections are suitable for the GTA (Global Thermal Aircraft) configuration which is part of the CRESCENDO (Collaborative & Robust Engineering using Simulation Capability Enabling Next Design Optimisation) project. Still, using the same process, one can design any other configuration, easily.

### A. Critical flight conditions

The critical flight conditions were considered for a vehicle weight of $W$ =11,840 kg (26,100 lb.) and typical wing area of $S_{wing}$ =30 m$^2$. The maximal lift coefficient is $C_{Lmax}$ = 1.7, maximum never exceed Mach number is $M_{NE}$ = 0.83, maximum altitude is $H_{max}$ = 37,000, and maximum airspeed at sea level, standard atmosphere (the maximal dynamic pressure limitation) is $V_{SL,ISA}$ = 300 kt. These parameters are used to determine the flight envelope of the air-vehicle as described in Fig. 15. This figure presents a Mach – Altitude chart of the ISA+20 deg flight envelope.

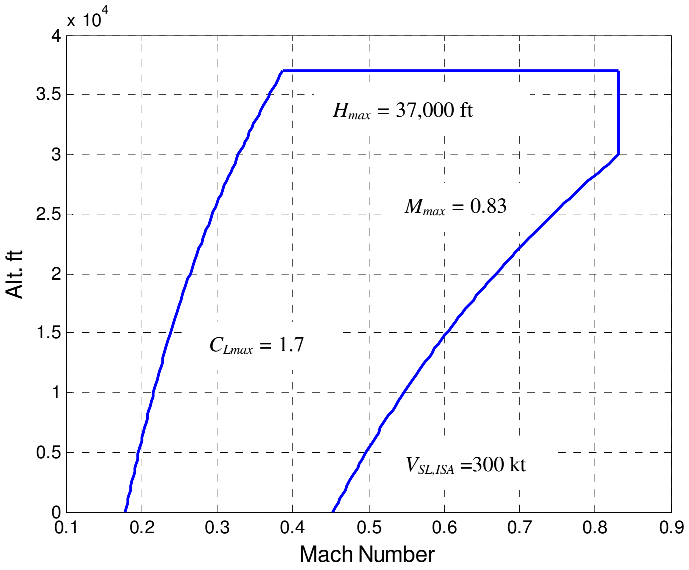

**Figure 15. Maximum and minimum temperature-ratio flight envelopes, ISA+20**

The critical conditions were calculated for initial compartment design, *i.e.* given inlet, ejector, and thermal model geometry. Table 3 contains the initial parameters which were used for the critical condition search. Other parameters were mentioned above in section III. One can notice that the inlet cross section is almost square and the mixing length is reduced to minimum.

**Table 3. Nominal parameters of inlet and ejector for the critical conditions calculation**

| Parameter | Initial Value |
|---:|:---|
| Inlet Width, $W_1$ | 0.4 m (1.3 ft) |
| Inlet Height, $D_1$ | 0.35 m (1.15 ft) |
| Orifice ratio, $F_{\text{Orifice}}$ | 0.275 |
| Exit of ejector mixing section area, $A_{10}$ | 0.113 m$^2$ (1.22 ft$^2$) |
| Mixing length, $L_{mix}$ | 0.0003 m (0.001 ft) |

Using these parameters and the framework of the first step (Step I in Fig. 3) of the design process, the temperature distribution at each flight condition can be calculated. A full factorial search is done over the entire flight envelope containing a grid of 46 altitudes and 27 Mach numbers. This makes a total of 1242 analyses which last on a desk-top computer an over night run (~8 hrs.). The authors aware that several improvements can accelerate this design step such as:

a. Using a coarser full-factorial grid
b. Parallelizing the full-factorial search
c. Introducing an optimization scheme instead of full-factorial search

Still, due to the relatively low computer resources needed in the current process, a simple high-density full-factorial approach is used.

Figure 16 shows the maximum normalized temperature ratio on the Mach-altitude flight envelope which is defined in Eq. (6). The right chart in Fig. 16 contains an enlargement of the critical condition region. It can be noticed that the critical conditions is at $H$ = 11,400 ft and $M$ = 0.22, on the low-velocity (stall) limit of the flight envelope. At these conditions the mass flow through the inlet is low thus, the temperatures levels are increased.

Figures 17 - 19 show the maximum temperature for the Aluminum nodes, Titanium nodes, and bay-flow nodes, respectively. Comparing these figures to Table 2 reveals that the critical conditions are caused by the Aluminum nodes. A closer examination reveals that the critical nodes are the fuselage rib which contacts the skin near the APU compartment nozzle. Figure 20 shows the thermal model results for the critical flight conditions. The APU exhaust flow, containing hot gasses, smears on the fuselage skin and heats the aluminum parts to high temperatures.

The compartment mass flow at the critical flight condition is 1.2 lb/sec (0.54 kg/sec) and the APU-engine mass flow is 2.1 lb/sec (0.95 kg/sec). This makes the total mass flow through the inlet 3.3 lb/sec (1.5 kg/sec). To examine the influence of the mass flow over the APU compartment temperature, various mass flows were run at the critical design conditions. The normalized temperature ratio is presented in Fig. 21. It is noticeable that the limit of the mass flow, thus obtaining a zero ratio, is 1.7 lb/sec (0.77 kg/sec). Figure 22 shows the maximum temperature for each material (Aluminum, Titanium and Bay Flow). According to Fig. 22 the limitation is due to the Aluminum nodes. To ensure that sufficient mass flow is available, a safety factor of 1.4 is used, thus, a mass flow of 2.4 lb/sec (1.1 kg/sec) is required. This value will be used as a design constraint in the next step (Step-II) phase of the design.

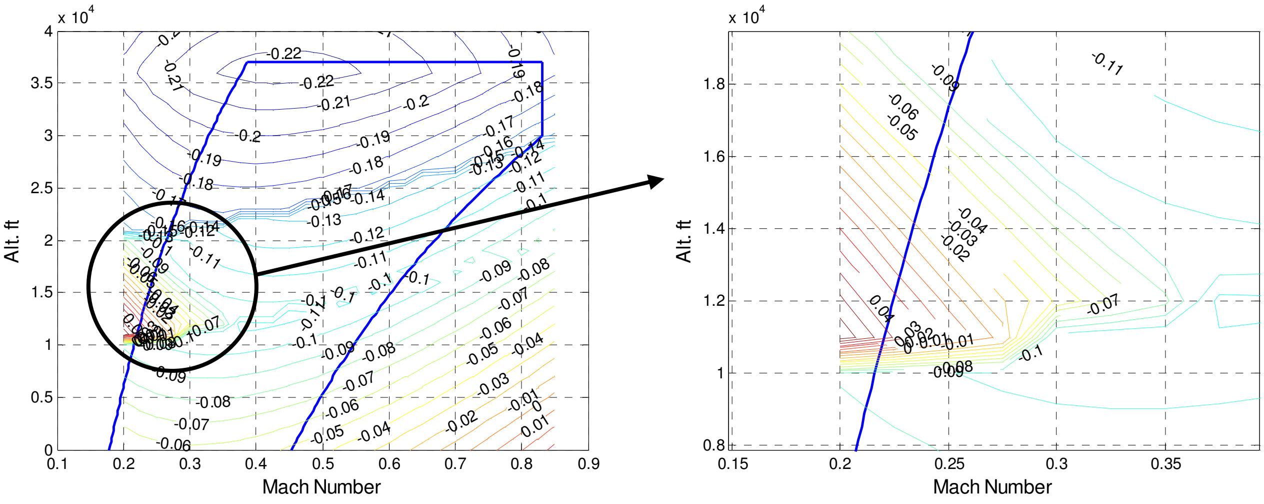

**Figure 16. Initial design Step-I results (Flight Conditions), normalized, maximum temperature ratio**

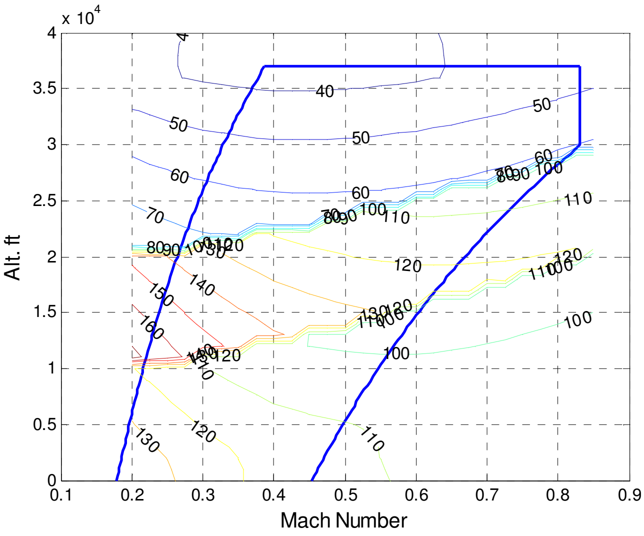

Figure 17. Initial design Step-I results (Flight Conditions), Aluminum maximum temperature, Centigrade

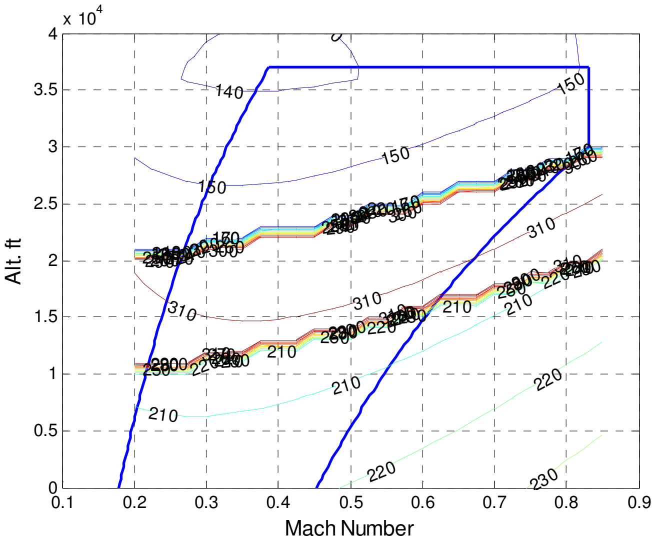

Figure 18. Initial design Step-I results (Flight Conditions), Titanium maximum temperature, Centigrade

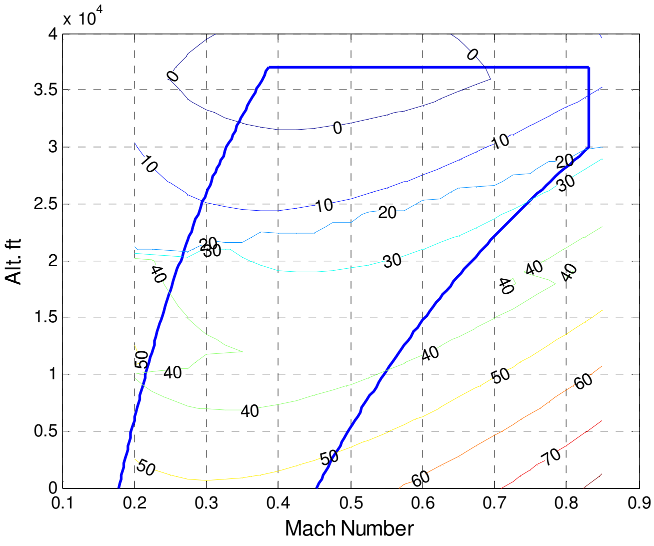

Figure 19. Initial design Step-I results (Flight Conditions), Bay-flow maximum temperature, Centigrade

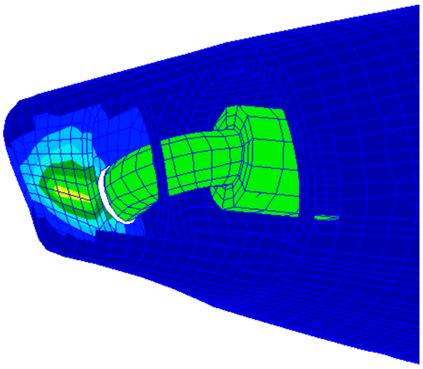

**Figure 20.** **SINDA results for the critical flight condition. The highest temperature is occurred on the aluminum skin which is affected by the hot exhaust gases.**

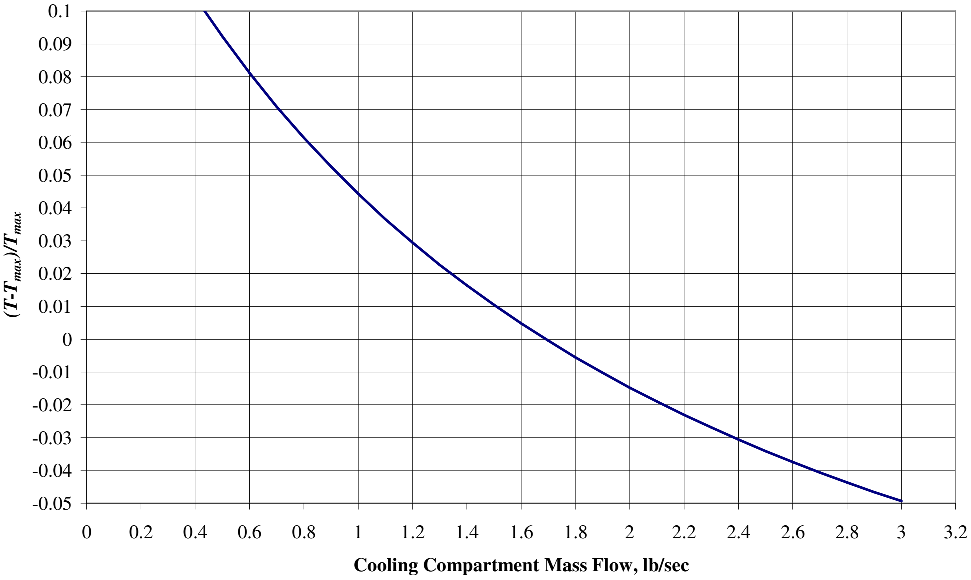

**Figure 21.** **Maximum normalized temperature ratio vs. APU compartment mass flow, at critical flight condition**

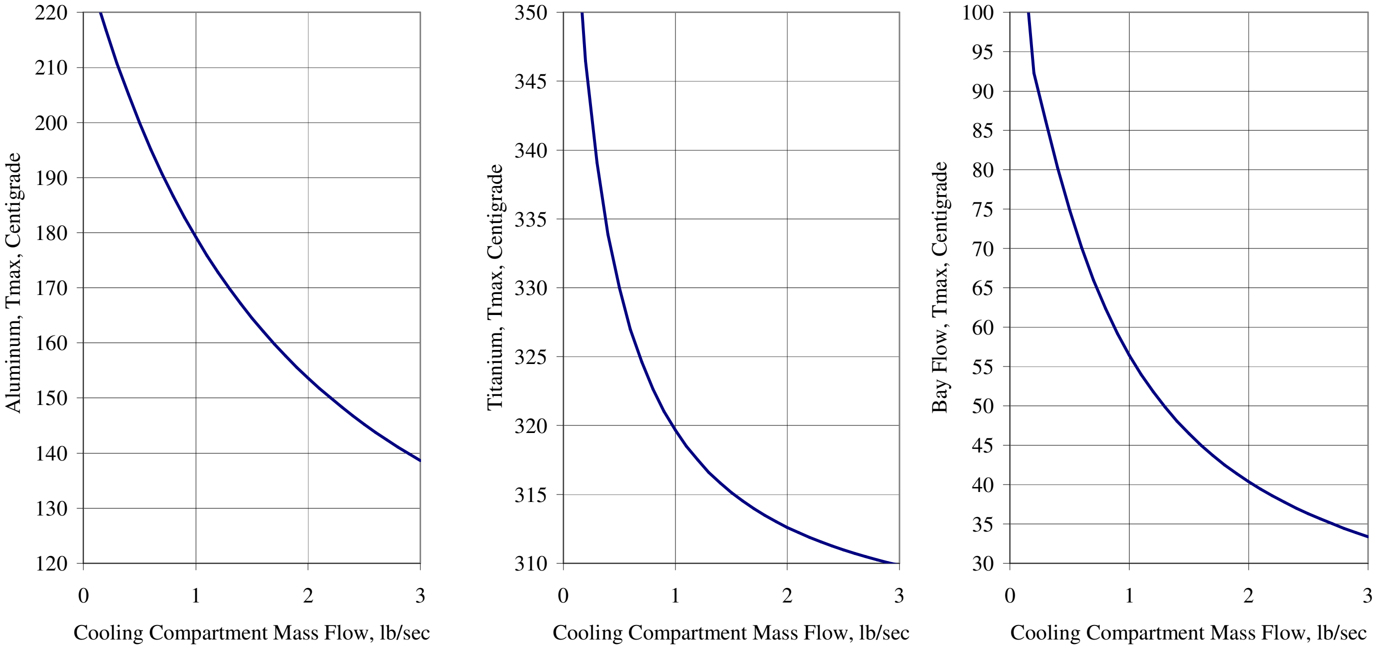

**Figure 22.** **Maximum temperature of the various materials vs. mass flow, at critical flight condition**

### B. Optimal inlet and compartment design

The critical design conditions found in the previous section are used to design the inlet and APU compartment geometry. This design is done using optimization scheme which is part of the modeFRONTIER design framework.

For the current effort five design variables were used (as mentioned in Table 3): the inlet width, $W_1$, and depth, $D_1$; the orifice ratio $F_{\text{Orifice}}$, ejector mixing length, $L_{mix}$, and the exit of ejector mixing section area, $A_{10}$. The other design parameters were kept fixed according to the nominal design. The parameters tolerance is given in Table 4. Figure 23 presents the design variables and their range in schematic manner.

**Table 4. Design variables tolerance**

| Design Variable | Min. Value | Max. Value |
|---:|:---:|:---:|
| Inlet Width, $W_1$ | 0.3 m (1.0 ft) | 0.5 m (1.65 ft) |
| Inlet Height, $D_1$ | 0.1 m (0.33 ft) | 0.4 m (1.31 ft) |
| Orifice ratio, $F_{\text{Orifice}}$ | 0.1 | 0.5 |
| Exit of ejector mixing section area, $A_{10}$ | 0.085 $m^2$ (0.9 $ft^2$) | 0.23 $m^2$ (2.5 $ft^2$) |
| Mixing length, $L_{mix}$ | 0.001 m ($3\times10^{-4}$ ft) | 0.25 m (0.0762 ft) |

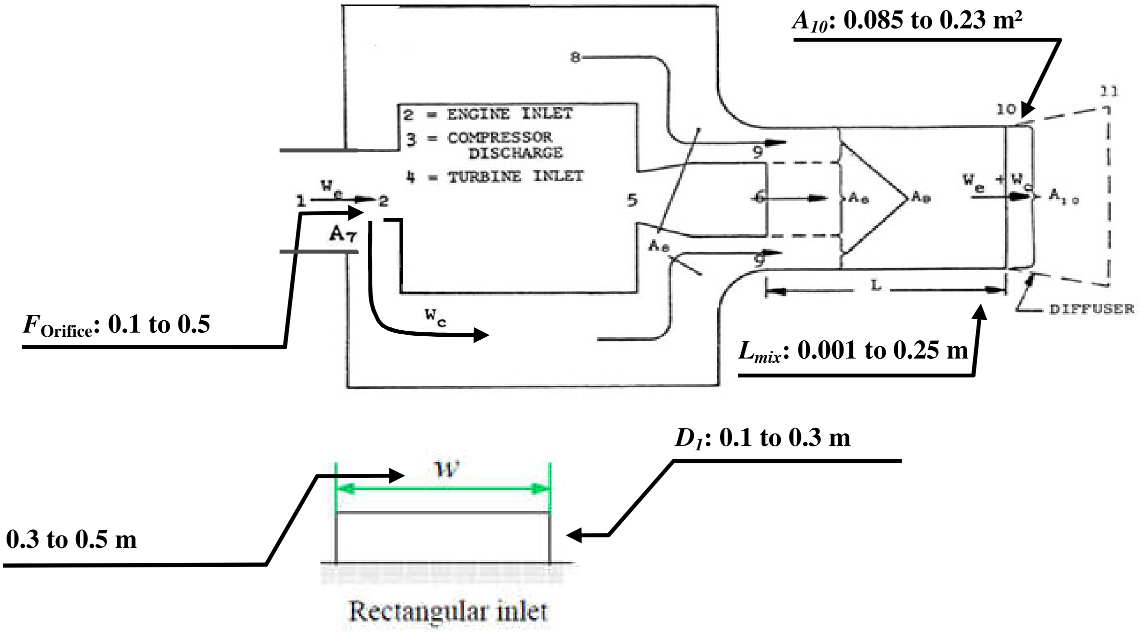

**Figure 23. Design variables definition**

Two design goals are used: the drag force produced by the inlet and the resulted mass flow at the APU compartment. The former is minimized while the latter is maximized. This multi-goal optimization is resulted with Pareto frontier pattern, thus the trade-off between the two goals can be examined.

modeFRONTIER enables the usage of several optimization schemes which suite multi-goal problems. In the current case an improved multi-objective genetic algorithm (MOGA) procedure is used. [10] The use of genetic algorithm enables a global search, thus it can overcomes the problem of local minima.[11] In a non-linear, non-convex design space, existence of large number of local minima may cause gradient based methods to be caught in local minima. Another reason of using MOGA is its capabilities with noisy optimization problems. [12]

Figures 24 shows the resulted Pareto fronts with the mass flow as horizontal axis and drag penalty as vertical axis. The Pareto front is a min-max shape, thus the required design is at the lowest right corner. The tradeoff between the drag penalty and the mass flow is noticeable and for a mass flow of 2.4 lb/sec (1.1 kg/sec) the drag penalty is not lower than 90 N. Although this value is not high, the trend is important for the following reasons:

a. Low drag penalty, at the critical flight conditions (low Mach number), can imply on much higher penalty for cruising at high Mach number. This will be shown in the following section.
b. Even small drag decrease can cause a substantial fuel saving during aircraft life cycle

In Fig. 24 the bubble color represents the inlet height, $D_1$, and the bubble diameter the inlet width, $W_1$. It is noticeable that for low drag (going vertically down) the inlet height is decreased and for high mass flow (going horizontally right) the inlet width is increased.

Figure 25 shows the same Pareto frontier but with the mixing length, $L_{mix}$, as the bubble color, and exhaust area, $A_{10}$, as the bubble diameter. For higher mass flow higher exhaust area is required. The mixing length trend is not unique. To demonstrate the relevance of the design variables a linear correlation chart is presented in Fig. 26. This chart represents the linear correlation of each variable with the other variables and the design goals. For values of 1 and -1 a full linear or inverse relation exists, respectively. For values closer to zero, no correlation is found. The mixing length correlation with both the drag and mass flow is low: 0.123 and -0.237, respectively. On the other hand the correlation of the inlet height with the drag is high: 0.835. The correlation of the inlet width with both drag and mass flow is relatively high. As mentioned above, these conclusions are evident also in the Pareto frontier charts (Figs. 24 and 25).

Another way of correlation inquiry is given in Figs. 27 and 28. In these figures all the designs which were calculated are given in a chart. Its vertical axis is the orifice ratio, $F_{Orifice}$, and the horizontal axis is the mass flow (Fig. 27) or drag penalty (Fig. 28). In Fig. 27 a distinctive lower bound represents the good correlation between the increased mass flow and increased orifice ratio. This can also be resolved from the correlation chart in Fig. 26 which gives a correlation of 0.895 between the orifice ratio and the mass flow. Figure 28 on the other hand, shows relatively low correlation between the orifice ratio and the drag penalty which again can be found in the correlation chart – 0.25 .

Examining the entire result give a solution which enable a 2.4 lb/sec of mass flow and minimized the drag penalty. Table 5 gives numerical values for the chosen design along with the initial design and the design variable range. The optimized design is superior to the initial design. It enables twice more of the mass flow through the APU compartment with half of the drag.

**Table 5. Resulted optimal design**

| Parameter | Initial | Range | Optimized |
|---:|:---:|:---:|:---:|
| Inlet Width, $W_1$, m | 0.4 | 0.3÷0.5 | 0.405 |
| Inlet Height, $D_1$, m | 0.35 | 0.1÷0.4 | 0.1 |
| Orifice ratio, $F_{\text{Orifice}}$ | 0.275 | 0.1÷0.5 | 0.5 |
| Exit of ejector mixing section area, $A_{10}$, m$^2$ | 0.113 | 0.085÷0.23 | 0.22 |
| Mixing length, $L_{mix}$, m | 0.001 | 0.001÷0.25 | 0.0385 |
| Mass flow, kg/sec | 0.5 | - | 1.09 |
| Drag, N | 206 | - | 92 |

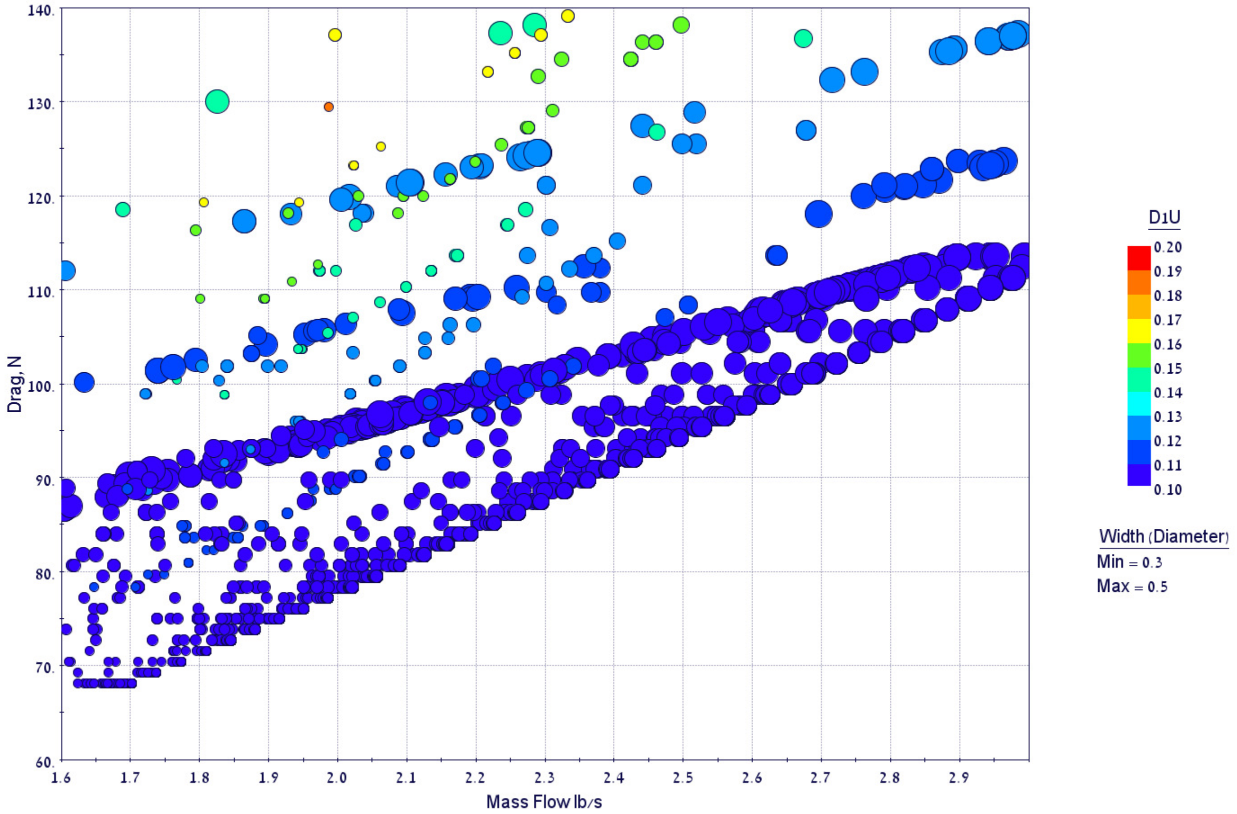

**Figure 24.** Pareto front of the drag force and mass flow. Color represents the inlet height, $D_1$, and bubble diameter the inlet width, $W_1$

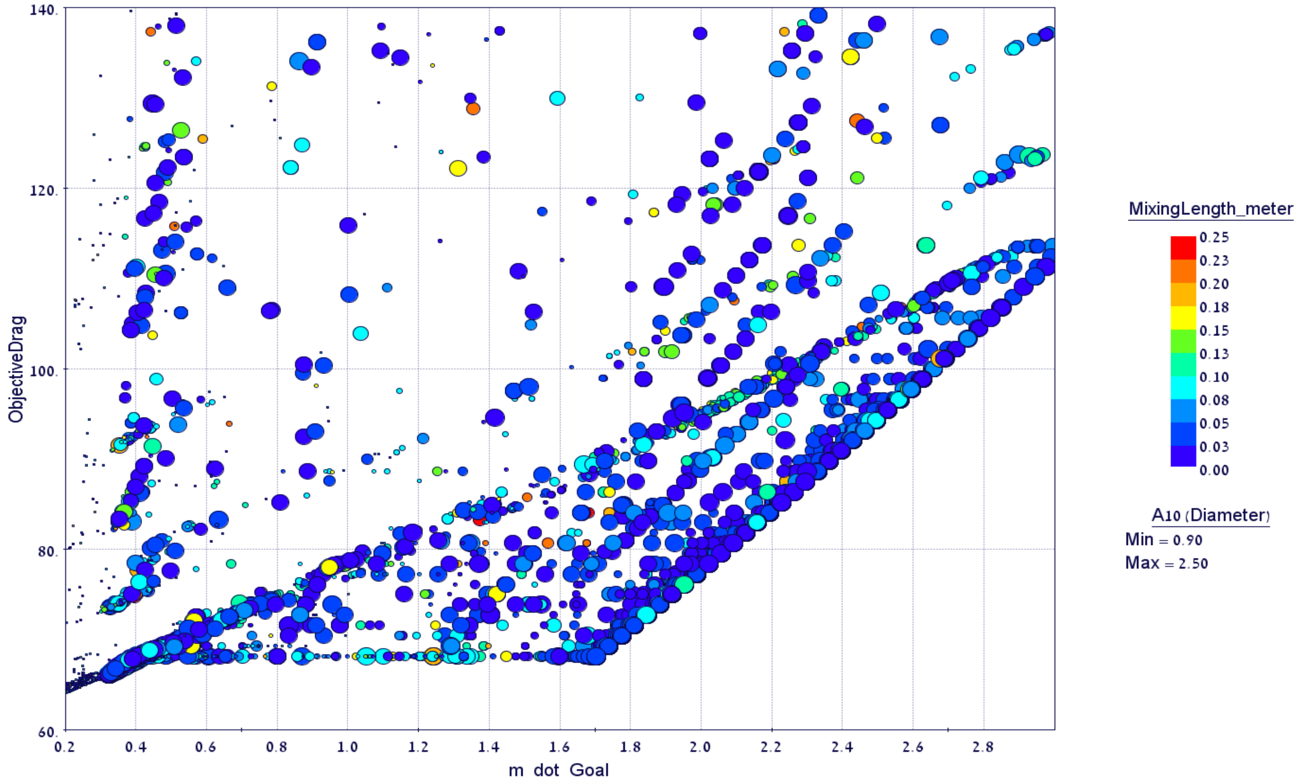

**Figure 25.** Pareto front of the drag force and mass flow. Color represents the mixing length, $L_{mix}$, , and bubble diameter the exhaust area, $A_{10}$

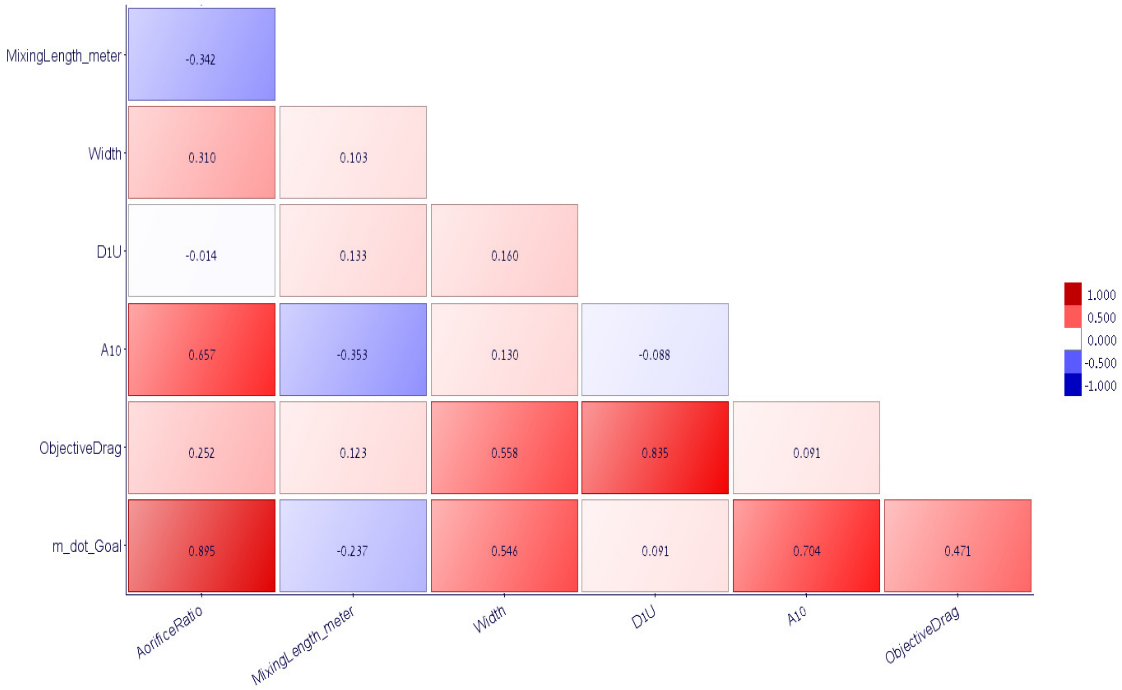

**Figure 26. Linear correlation of the design variables and design goals**

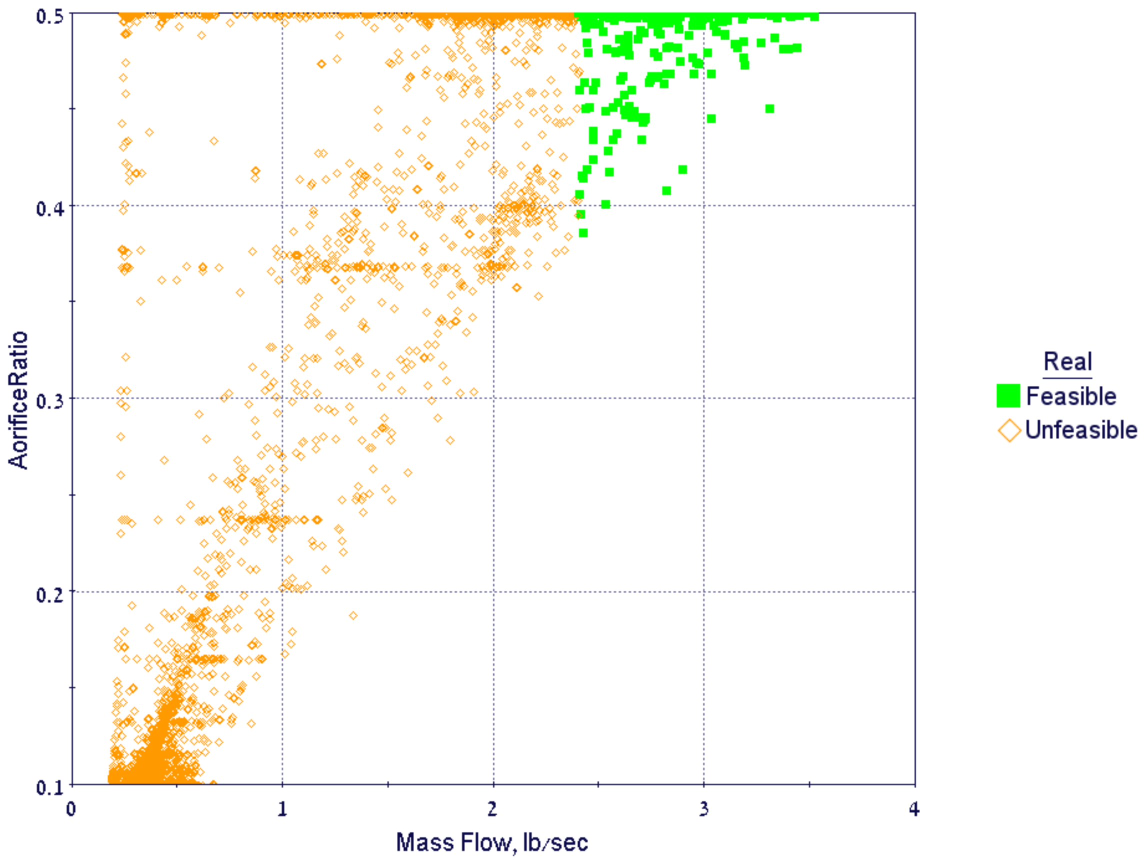

**Figure 27. Resulted designs: orifice ratio, $F_{\text{Orifice}}$, vs. mass flow.**

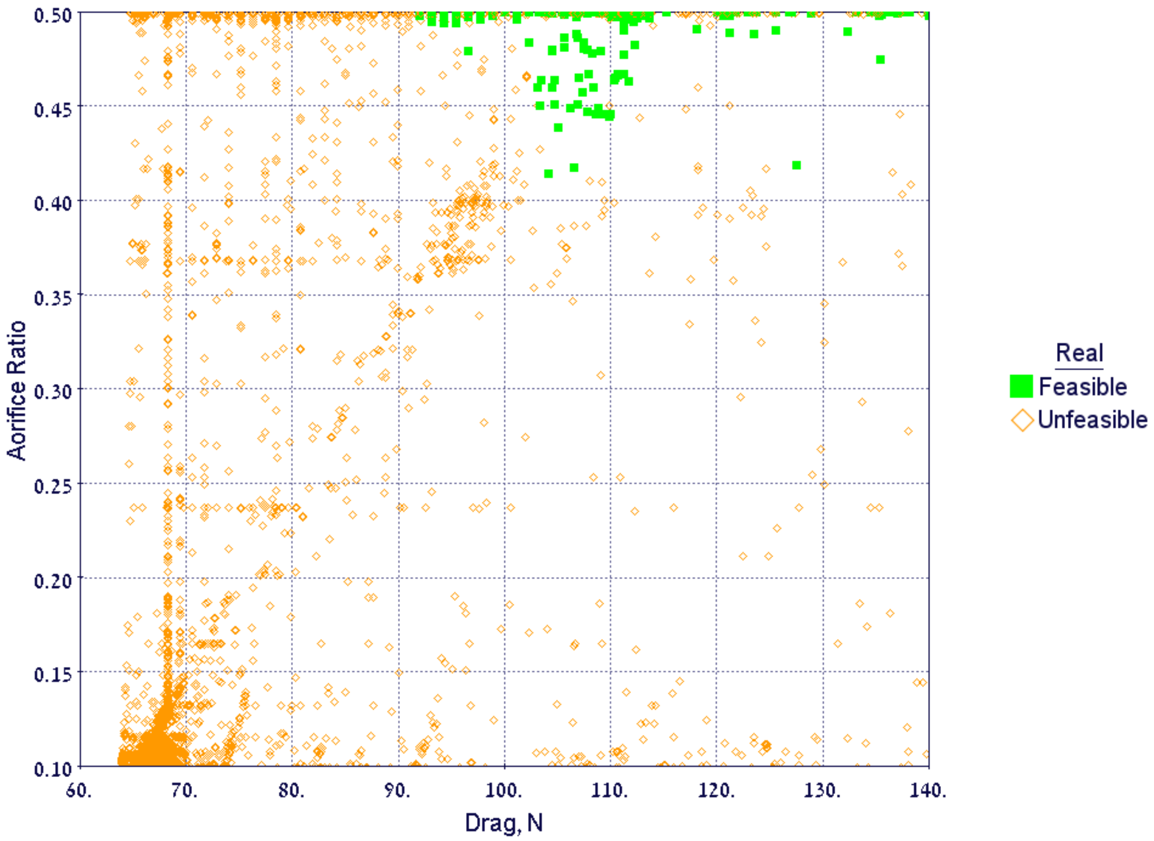

**Figure 28. Resulted designs: orifice ratio, $F_{\text{Orifice}}$, vs. drag penalty**

### C. Design Loop Closure

To validate the quality of the optimized design found in the previous section, the flight envelope temperature distribution is run again. This is done by repeating Step-I procedure (Fig. 3), but now with the optimized design parameters (Table 5). The optimized design parameters were used to re-model the thermal model and re-mesh it, thus, generating an updated thermal model, which represents the optimized design. Figure 29 compares between the initial and optimized geometry of the thermal model. Note that this was the only remodeling done with the thermal model, thus, it can be conducted manually without generating sophisticated automatic modeling and meshing capability.

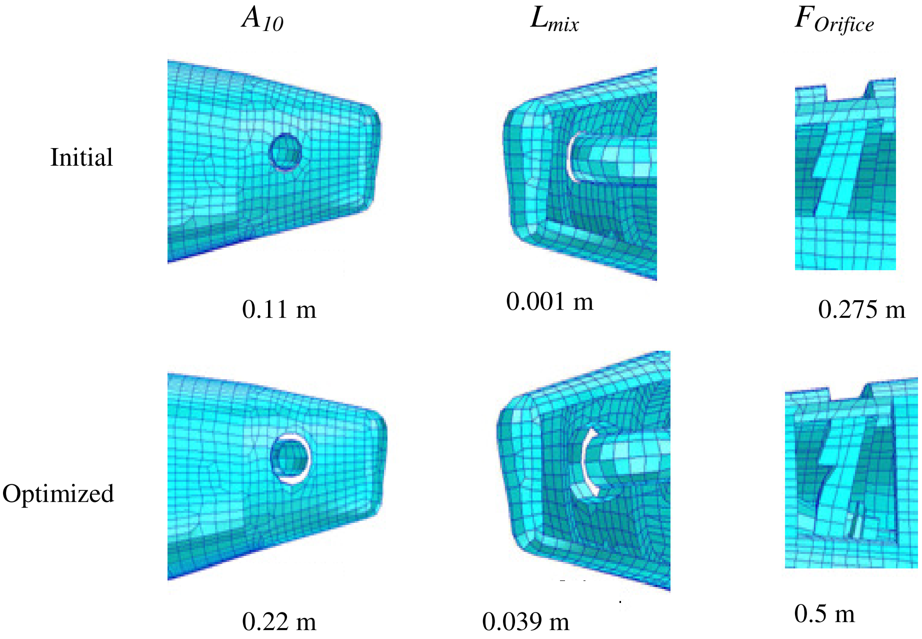

**Figure 29. Updating the thermal model geometry according to optimized design**

Figure 30 shows the resulted normalized temperature ratio. Comparing to the same chart, but for the initial design (Fig. 16) reveals the improvement of the design. In addition, it is noticeable that the critical conditions are maintained the same as in the initial design, while the entire flight envelope contains negative temperature ratio. Thus, the optimized design is validated as a suitable design which maintains its temperature level below the material limits.

Figure 31 compare between the drag penalties at the entire flight envelope, of the initial design versus the final optimized design. It shows that the drag drops by a factor of 2. For the current air-vehicle, which weights 11,840 kgf, and an estimated lift-to-drag ratio at cruise of 15, the drag is about 8,000 N. A decrease of 500 N at the high Mach number regime is equivalent to more than 6% decrease of the total vehicle drag. This amount of drag reduction is significant and may contribute dramatically to the air-vehicle performance.

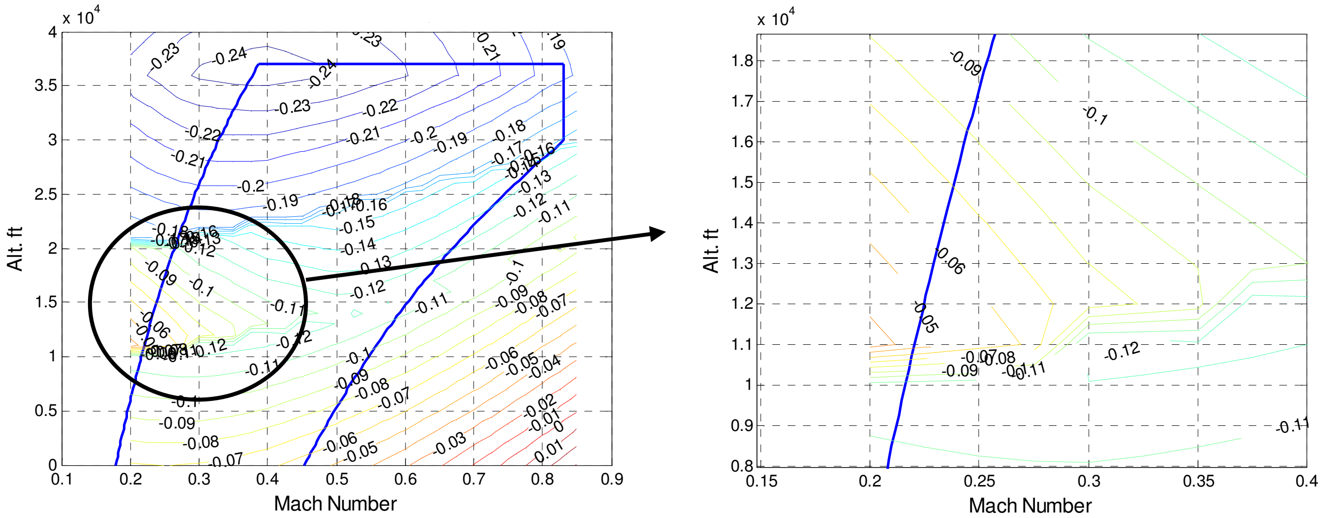

**Figure 30. Optimized design Step-I results (Flight Conditions), normalized, maximum temperature ratio**

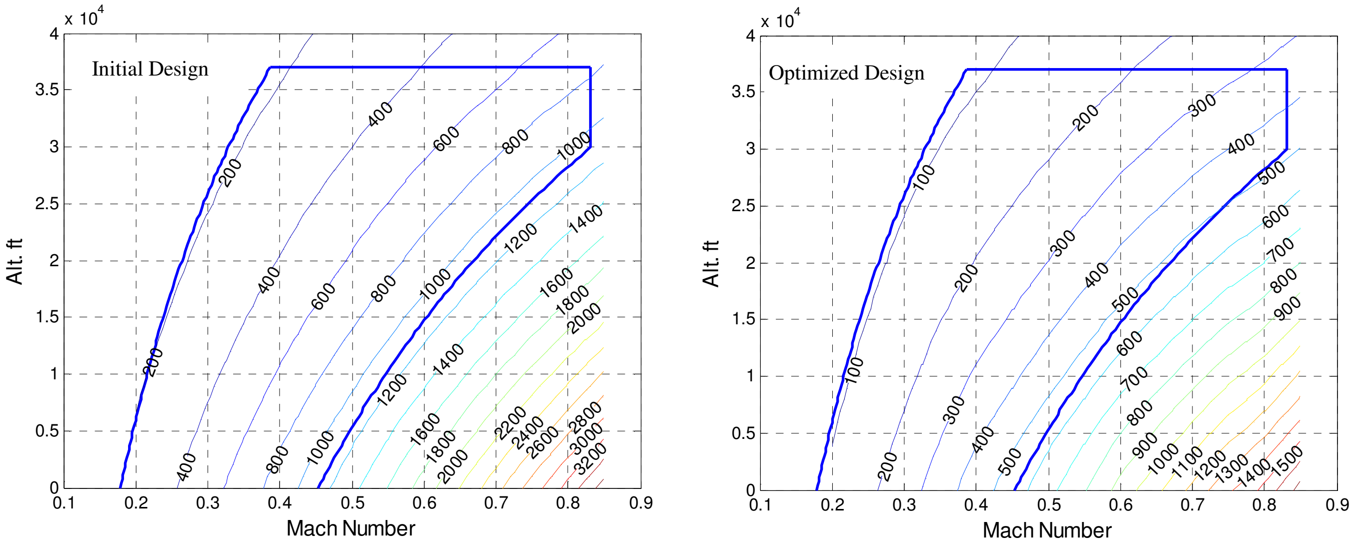

**Figure 31. Comparison of initial and optimized design.**
**Step-I results (Flight Conditions), drag penalty, N**

# V. Conclusions

The above paper reviews the design process for an APU compartment. The design includes several models such as the inlet, APU-engine, 1-D flow and ejector, and thermal model. Integration of all these models into single design process enables the search for an optimized design.

The use of design environment such as ESTECO modeFRONTIER enables an easy integration of the model components into a synergetic design framework. In addition, the framework supplies advance tools for a multi-objective optimization which results with an optimized Pareto frontier. This is then used by the decision makers to establish their tradeoff between contradicting design goals by choosing a design which lies on the Pareto frontier.

The design process is divided into two separate steps, thus a bi-level design process is developed. This uses the higher fidelity thermal model just for the critical flight condition estimation and enables the use of other low fidelity models for the geometric optimization of the compartment. The absence of re-modeling and re-meshing of the thermal model saves computer resources. The thermal model is remodeled and re-meshed only once during the design process. This single perturbation is conducted to validate the final design. This design process should be monitored carefully. It is possible that the validation process will fail and the entire design sequence will restart, although the design sequence is relatively short.

Usage of the low fidelity models decreases the required computer resources. In addition, the framework is very flexible and can be easily modified. The low-fidelity models can be shared with other partners and it does not require license nor large computer resources. Still, the implementation of thermal analysis in a preliminary design procedure is important and it reduces uncertainties in the more advance design phases.

The above described methodology guides the designer to predetermined design goals and proof of concept. By doing so, the resulted APU-compartment design features an increased air mass flow thus an increased cooling efficiency. On top of that the inlet drag penalty is reduced dramatically by more than 50%, compared to the initial design. Note that this initial design was chosen arbitrarily. It is possible that for a better initial design, the improvement will be more modest.

Although the current design process is developed for an APU-compartment design, it can be used for any other design involving the basic building blocks (*i.e.* inlet, 1-D flow, thermal model, etc.). By implementing other models such as empirically based or CFD solvers, the design authority can be increased even further, to other disciplines, and the knowledge regarding the design can be increased during the conceptual and preliminary design phases.

## Acknowledgment

The research has received funding from the European Union Seventh Framework Program (FP7/2007-2013), URL: www.crescendo-fp7.eu/

## Reference:

[1] E. Harris and Staff, "Design of H2-O2 space shuttle APU," NASA CR-121214, January 1974.

[2] D. Gorinevsky. K. Dittmar, D. Mylaraswamy, and E. Nwadiogbu, "Model-based diagnostics for an aircraft auxiliary power unit," IEEE Conference on Control Applications, Glasgow, Scotland, 18-20 September, 2002.

[3] G.G. Ordonez, and M. J. Georges, "Aircraft performance sensitivities to ejector nozzle concepts," AIAA 91-3135*, AIAA Aircraft design Systems and Operations Meeting*, Baltimore Maryland, 23-25 September, 1991.

[4] A. B. Jesus, and G. L. Oliveira, "A methodology for the design of APU air inlets for regional commercial aircraft," AIAA 2003-722, *41st Aerospace Science Meeting and Exhibit*, Reno Nevada, 6-9 January 2003,

[5] C.W.Frick, W.F.Davis, L.M.Randall, and E.A.Mossman, "An experimental investigation of NACA submerged-duct entrances," NACA ACR No. 5120, October 1945.

[6] The Royal Aeronautical Society, "Drag and pressure recovery characteristics of auxiliary air inlets at subsonic speeds," ESDU 86002, April 1986

[7] SAE International, "Performance of low pressure ratio ejectors for engine nacelle cooling," *SAE Aerospace Information Report*, AIR-1191 Rev. A, March 1993.

[8] M. Thomas, "Presentation: auxiliary power unit model, CRESCENDO S2T1," AIRBUS, September 2010.

[9] MIL-HDBK-5400, "Military handbook: electronic equipment, airborne, general guidelines for," 30 November, 1995.

[10] S. Poles., "MOGA-II an improved multi-objective genetic algorithm," Technical report 2003-006, Esteco, Trieste, 2003.

[11] Van der Velden A., “Tools for applied engineering optimization”, AGARD R 803AGARD-FDP-VKI special course, April 1994

[12] S. Poles, E. Rigoni, T.Robič, "MOGA-II performance on noisy optimization problems," BIOMA 2004, International Conference on Bioinspired Optimization Methods and Their Applications, Ljubljana, Slovania, October 11-12, 2004.

View publication stats